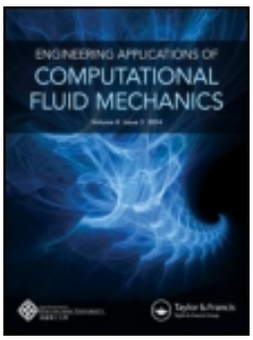

Engineering Applications of Computational Fluid Mechanics

ISSN: 1994-2060 (Print) 1997-003X (Online) Journal homepage: http://www.tandfonline.com/loi/tcfm20

Comparative study of buoyancy-driven instability for thermohaline stratification in a Hele-Shaw cell and extended geometry

Yingying Luo & Yejun Gong

To cite this article: Yingying Luo & Yejun Gong (2015) Comparative study of buoyancy-driven instability for thermohaline stratification in a Hele-Shaw cell and extended geometry, Engineering Applications of Computational Fluid Mechanics, 9:1, 469-476, DOI: 10.1080/19942060.2015.1066533

To link to this article: http://dx.doi.org/10.1080/19942060.2015.1066533

Engineering Applications of Computational Fluid Mechanics, 2015
Vol. 9, No. 1, 469–476, http://dx.doi.org/10.1080/19942060.2015.1066533

Taylor & Francis
Taylor & Francis Group

Comparative study of buoyancy-driven instability for thermohaline stratification in a Hele-Shaw cell and extended geometry

Yingying Luo and Yejun Gong*

Department of Applied Mechanics and Engineering, Sun Yat-sen University, Guangzhou, China

(*Received 2 February 2015; final version received 4 June 2015*)

Studies on buoyancy-driven instabilities are of considerable interest for its wide application in oceanic, environmental and industrial fields. For miscible two-layer stratifications in a Hele-Shaw cell, the base state density profile in the diffusion regime can be predicted by linear stability analysis such that the buoyancy-driven instabilities can be classified in (R, δ) parameter space, where R is the initial density stability ratio and δ is the diffusion coefficient ratio. However, flow dynamics in extended geometry do not satisfy Darcy's law. Hence, linear stability analysis cannot be applied to unbounded flow with nonlinear momentum convection. In this study, we carry out a series of numerical simulations to investigate buoyancy-driven instability for thermohaline stratification in both a Hele-Shaw cell and extended geometry at a high thermal Rayleigh number, $Ra_T = 7 \cdot 10^6$, with $R = 0.05$, 0.25, 0.8, 1, 4, and 20. The time evolution of the density stability ratio, temperature, salinity and base state density are calculated and compared. Fingers of unbounded thermohaline stratification have a more distorted shape due to the nonlinear momentum convection. However, the base state density profile of thermohaline stratification in extended geometry is found to be similar to that of a Hele-Shaw cell; thus, the classification of buoyancy-driven instabilities in (R, δ) space for miscible two-layer stratifications in Hele-Shaw cells can be extended to the same flow in extended geometry.

Keywords: Buoyancy-driven instability; salt finger; classification

Introduction

During the mixing of two miscible fluids, the buoyancy-driven instabilities influence mass and heat transportation in CO_2 sequestration, soil contamination, stellar dynamics and chemical engineering, among others. The well-known Rayleigh-Taylor (RT) instability occurs when a denser solution lies on top of a less dense one (Sharp, 1983). Another highly interesting buoyancy-driven instability is the double-diffusive (DD) instability, which happens when two different variables are diffusing at different rates – e.g., the hot salt water located above the cold fresh water in the ocean, with temperature as the fast diffuser and salinity as the slow diffuser – and this instability mode leads to the famous 'salt finger' phenomenon (Radko, 2008). Buoyancy-driven instability has attracted great interest for its influence on heat and mass transfer (Li, Zhan, & Luo, 2008).

The buoyancy-driven instabilities of two miscible fluids in a porous medium or a Hele-Shaw cell have been classified systematically in (R, δ) parameter space, where R is the density stability ratio and δ is the diffusion coefficient ratio. In the related research (Mishra, Trevelyan, Almarcha, & De Wit, 2010; Rongy, Trevelyan, & De Wit, 2010; Trevelyan, Almarcha, & De Wit, 2011), the upper solution contains a species A in a concentration A_0 with a diffusion coefficient D_A and expansion coefficient α_A, whilst the lower solution contains a solute B in a concentration B_0 with a relative D_B and α_B. Then the density stability ratio R and the diffusion coefficient ratio δ are defined as follows:

$$R = \frac{\alpha_B B_0}{\alpha_A A_0} \quad \text{and} \quad \delta = \frac{D_B}{D_A}. \tag{1}$$

The Hele-Shaw cell is composed of two glass plates separated by an infinitesimally thin gap. The governing equations for the miscible two-layer fluids in a Hele-Shaw cell follow Darcy's law, as with the flow in a porous medium. Hence, Hele-Shaw cells are widely used in the laboratory to visualize the two-dimensional flow in a porous medium (Fernandez, Kurowski, & Petitjeans, 2002; Griffiths, 1981; McLean & Saffman, 1981). For the miscible two-layer flow in a Hele-Shaw cell, the nonlinear momentum equation can be linearized such that the linear stability analysis is able to predict the density profile in base state following diffusive dynamics, and the classification of buoyancy-driven instability is developed upon the base state density profile (Carballido-Landeira, Trevelyan, Almarcha, & De Wit, 2013; Trevelyan et al., 2011). For $R < 1$, the density of the upper solution $\rho_A = \rho_0$

*Corresponding author. Email: yejungong@126.com; gongyj3@mail.sysu.edu.cn

$(1+\alpha_A A_0)$ is greater than the density $\rho_B = \rho_0(1+\alpha_B B_0)$ of the lower solution, where ρ_0 denotes the density of the pure solvent. Then the less dense fluid rises between the sinking denser fluid, and the interface deforms into 'density fingering' due to the so called RT instability. For $R > 1$ and $\delta > 1$, the species B in the lower and heavier solution diffuse upward faster than the species A, and 'salt fingering' occurs for this DD instability. For $R > 1$ and $\delta < 1$, the system remains undisturbed for a while, and then the diffusive-layer convection (DLC) occurs because of the differential diffusion effect. Numerical simulations of the miscible two-layer flow with species A and B ($\delta = 0.3$ or 3) have been carried out to confirm the validation of linear stability analysis (Carballido-Landeira et al., 2013; Trevelyan et al., 2011).

However, the flow dynamics of unbounded miscible two-layer stratification does not obey Darcy's law, such that the linear stability analysis cannot be applied to unbounded two-layer stratifications. Hence, it remains uncertain whether the classification of buoyancy-driven instabilities based on linear stability analysis can be extended to the unbounded stratification. Note that, 'unbounded' flow in 'extended geometry' refers to the flow which is not confined by two glass plates, as in a Hele-Shaw cell.

The thermohaline stratification is a typical unbounded miscible two-layer flow in nature (Griffiths, 1981). Here, we focus on the thermohaline stratification with hot salt water located above cold fresh water. The two dimensionless parameters, R and δ, are always given in the following form:

$$R = R_{\rho 0} = \frac{\alpha_T \Delta T}{\alpha_S \Delta S}, \text{ and } \delta = Le = \frac{D_T}{D_S}, \tag{2}$$

where T is the temperature, S is the salinity, $R_{\rho 0}$ denotes the initial value of the time-dependent density stability ratio $R_\rho(t)$, and Le denotes the dimensionless Lewis number. Then the value of δ is about 100 in heat-salt system. The effect of the initial density stability ratio R on thermohaline stratification ($\delta = 100$) has been investigated experimentally and numerically (Stern & Radko, 1998; Yoshida & Nagashima, 2003). When $R < 1$, thermohaline stratification is gravitationally unstable, and 'density fingers' appear due to RT instability (Singh & Srinivasan, 2014); when $1 < R < \delta$, the well-known 'salt fingering' phenomenon occurs for thermohaline stratification in extended geometry due to DD instability (Stern, 1960). Additionally, certain rules exist for the dynamics of 'salt fingers': if $R_\rho \to \delta$ then the salt fingers turn into slim filaments, heat transfer in the vertical direction is small, and the flow is nearly laminar and can be explained by weakly nonlinear instability theory (Radko & Stern, 2000); if $R_\rho \to 1^+$then the salt fingers split into isolated droplets, the vertical temperature and salinity fluxes are enhanced significantly, and the flow is more turbulent and governed by secondary super-exponential instabilities (Radko, 2008; Stern & Simeonov, 2005).

In this study, numerical simulations of the thermohaline stratification ($\delta = 100$) with various density stability ratio R are performed, both in a Hele-Shaw cell and in extended geometry for a comparative study. The governing equations for thermohaline stratification in Hele-Shaw cells and in extended geometry are nondimensionalized using the same reference values, and the relative stream functions are resolved using a self-developed computational code. The density stability ratio, temperature, salinity and base state density profile are calculated for comparison.

Mathematical model

For the flow satisfying Boussinesq assumption, the fluid density depends linearly on the local temperature and salinity, i.e.,

$$\Delta\rho = \Delta\rho_T + \Delta\rho_S = \rho_0(-\alpha_T \Delta T + \alpha_S \Delta S), \tag{3}$$

where ρ_0 is the density of the pure solvent and $\alpha_T = -1/\rho_0[\partial\rho/\partial T]_S$ and $\alpha_S = 1/\rho_0[\partial\rho/\partial S]_T$ are the expansion coefficients of temperature and salinity, respectively. The incompressible thermohaline stratification is governed by the following equations:

$$\nabla \cdot \mathbf{U} = 0, \tag{4}$$

$$\frac{\partial \mathbf{U}}{\partial t} + \mathbf{U}\cdot\nabla\mathbf{U} = -\frac{1}{\rho}\nabla p_d + \nu\nabla^2\mathbf{U} - g(-\alpha_T\Delta T + \alpha_S \Delta S)\mathbf{j}, \tag{5}$$

$$\frac{\partial T^*}{\partial t} + \mathbf{U}\cdot\nabla T^* = D_T\nabla^2 T^*, \tag{6}$$

$$\frac{\partial S^*}{\partial t} + \mathbf{U}\cdot\nabla S^* = D_S\nabla^2 S^*, \tag{7}$$

where t, $\mathbf{X}$, $\mathbf{U}$, T^*, and S^* are the dimensional time, position, velocity, temperature, and salinity, respectively. The dynamic pressure is denoted as p_d and $\mathbf{j}$ is the unit vector in the vertical direction. The dimensional variables can be scaled as follows:

$$\mathbf{x} = \frac{\mathbf{X}}{H}, \mathbf{u} = \frac{\mathbf{U}}{D_T/H}, p = \frac{p_d}{D_T^2\rho_0/H^2}, \quad \tau = \frac{t}{H^2/D_T}, T = \frac{T^* - T_0^*}{\Delta T^*}, S = \frac{S^* - S_0^*}{\Delta S^*}, \tag{8}$$

where g is gravity, ν is the momentum diffusion coefficient (also known as the kinematic viscosity), τ is nondimensional time, $\mathbf{x}$ is the nondimensional position vector, $\mathbf{u}$ is the nondimensional velocity, T and S are the nondimensional temperature and salinity at the time τ, respectively, H is the height of the computation domain, T_0^* and S_0^* are

the initial temperature and salinity of the bottom layers, and ΔT^* and ΔS^* are the initial difference of temperature and salinity between the two layers. The dimensionless Prandtl number Pr and Schmidt number Sc are given as

$$Pr = \frac{\nu}{D_T}, Sc = \frac{\nu}{D_S}, \text{ and then } \delta = \frac{Sc}{Pr}. \tag{9}$$

Then the governing equations (4)–(7) can be nondimensionalized as follows:

$$\nabla \cdot \mathbf{u} = 0, \tag{10}$$

$$\frac{\partial \mathbf{u}}{\partial \tau} + \mathbf{u} \cdot \nabla \mathbf{u} = -\nabla p + Pr\nabla^2 \mathbf{u} + \left[PrRa_T \left(T - \frac{1}{R_\rho} S \right) \right] \mathbf{j}, \tag{11}$$

$$\frac{\partial T}{\partial \tau} + \mathbf{u} \cdot \nabla T = \nabla^2 T, \tag{12}$$

$$\frac{\partial S}{\partial \tau} + \mathbf{u} \cdot \nabla S = \frac{1}{\delta} \nabla^2 B, \tag{13}$$

where the Rayleigh numbers of the two components are given as,

$$Ra_T = \frac{g\alpha_T \Delta T H^3}{\nu D_T} \text{ and } Ra_S = \frac{g\alpha_S \Delta S H^3}{\nu D_S}. \tag{14}$$

The thermal Rayleigh number Ra_T determines whether heat transfer in a buoyancy-driven flow is governed by conduction or convection. When the thermal Rayleigh number is high ($Ra_T = 7 \cdot 10^7$ in this context), tiny noise perturbation would get intensified and probably induce overturning and instability of the system.

The governing equations (4)–(7) can be rewritten into stream function-vorticity form as follows:

$$\frac{\partial^2 \psi}{\partial x^2} + \frac{\partial^2 \psi}{\partial y^2} + \omega = 0, \tag{15}$$

$$\frac{\partial \omega}{\partial \tau} + \frac{\partial \psi}{\partial y}\frac{\partial \omega}{\partial x} - \frac{\partial \psi}{\partial x}\frac{\partial \omega}{\partial y} = Pr\left(\frac{\partial^2 \omega}{\partial x^2} + \frac{\partial^2 \omega}{\partial y^2} \right) + Pr \cdot Ra_T \left(\frac{\partial T}{\partial x} - \frac{1}{R_\rho}\frac{\partial S}{\partial x} \right), \tag{16}$$

$$\frac{\partial T}{\partial \tau} + \frac{\partial \psi}{\partial y}\frac{\partial T}{\partial x} - \frac{\partial \psi}{\partial x}\frac{\partial T}{\partial y} = \frac{\partial^2 T}{\partial x^2} + \frac{\partial^2 T}{\partial y^2}, \tag{17}$$

$$\frac{\partial S}{\partial \tau} + \frac{\partial \psi}{\partial y}\frac{\partial S}{\partial x} - \frac{\partial \psi}{\partial x}\frac{\partial S}{\partial y} = \frac{1}{\delta}\left(\frac{\partial^2 S}{\partial x^2} + \frac{\partial^2 S}{\partial y^2} \right), \tag{18}$$

where ψ and ω are the stream function and vorticity of the nondimensional velocity, respectively.

Based on Darcy's law, the momentum equation (equation (5)) for thermohaline stratification in a Hele-Shaw cell can be simplified as follows (Trevelyan et al., 2011):

$$\frac{1}{\rho}\nabla p_d = -\frac{\nu}{K}\mathbf{U} - g(-\alpha_T \Delta T + \alpha_S \Delta S)\mathbf{j}, \tag{19}$$

where K is the permeability, and it is defined as $K = a^2/12$, when the flow between the two layers is contained in a vertically-orientated Hele-Shaw cell with a narrow gap of width a. Then plug equation (8) into equation (19) and the result is

$$\nabla p = -Pr \cdot \Theta \mathbf{u} + Pr \cdot Ra_T (T - \frac{1}{R_\rho} S)\mathbf{j}, \tag{20}$$

where $\Theta = H^2/K$ is a dimensionless variable depending on the Hele-Shaw geometry. Note that equations (5) and (19) are nondimensionalized using the same reference values, which are different to those used in Trevelyan et al. (2011). Hence, the dimensionless equation (20) can be rewritten into the following stream function form:

$$\left(\frac{\partial^2 \psi}{\partial x^2} + \frac{\partial^2 \psi}{\partial y^2} \right) = -\frac{Ra_T}{\Theta}\left(\frac{\partial T}{\partial x} - \frac{1}{R_\rho}\frac{\partial S}{\partial x} \right) \tag{21}$$

We have carried out preliminary numerical experiments on the two-layer fluid system using the dual-mesh hybrid numerical method with the fast Poisson solver DFPS2H (double precision two-dimensioned fast Poisson solver) based on the high-order differences with identity expansion (HODIE) finite difference scheme (Zhan, Luo, & Li, 2008). The applied numerical methods have been validated using experimental data from our previous studies (Li et al., 2008; Zhan et al., 2008).

Computational setup

We consider a two-layer stratified system of thermohaline flow in a basin with a domain aspect ratio of 1:1 (x:y). The initial temperature and salinity are given as step functions with $T_0 = 1$ and $S_0 = 1$ on the top layer and $T_0 = 0$ and $S_0 = 0$ on the lower layer. All boundaries are adiabatic and impenetrable – that is, the gradient of the temperature and salinity are zero in the normal direction of all boundaries. The slip-velocity boundary condition is applied on all sidewalls and the no-slip condition is applied on the top and bottom walls. A structured mesh with the same grid number in horizontal and vertical directions is used to resolve the flow two-dimensionally. The mesh is refined near the interface, and the total grid number is 251 × 251 for all cases.

Numerical simulations will resolve the heat-salt system at the high thermal Rayleigh number $Ra_T = 6 \cdot 10^7$ with various density stability ratios of $R = 0.05, 0.25, 0.8, 1, 4$ and 20. The diffusion ratio of thermohaline stratification is $\delta = 100$ when hot salted water is on the upper layer. The new dimensionless variable, Θ in equation (20), is supposed to equal 10^4 for all Hele-Shaw flow cases in this context.

Results

Variation of density stability ratio

For miscible two-layer flow in a Hele-Shaw cell, Trevelyan et al. (2011) calculated the onset time of convection from a linear stability analysis. For thermohaline stratification, the numerical simulation results of Singh and Srinivasan (2014) show that the density stability ratio $R_\rho(t)$ decreases before the onset time and then increases monotonously, indicating that it is gravitationally more stable. We also observed the same tendency in the $R\rho(t)$ curve for both the Hele-Shaw cell and extended geometry, as shown in Figures 1(a) and 1(b), where $R_\rho(t)$ is divided by the initial value $R = R_{\rho 0}$ such that all $R\rho(t)$ curves can be configured in one picture.

The calculated onset time τ_o of each case is given in Table 1, and τ_o increases with the initial density stability ratio R. Here, thermohaline stratification with $R = 20$ remains in the diffusive regime until the end of the computation (almost fully mixed), so the onset time of this case is given as $\tau_o > 2.57e-02$ for the Hele-Shaw cell and $\tau_o > 3.68e-03$ for extended geometry.

Before the onset time of convection, $\tau \le \tau_o$, the heat-salt system is governed by molecular diffusion, no fingers appear on the initial interface between the two layers, and temperature diffuses much faster than the nearly unchanged salinity. Indeed, the temperature diffusion coefficient is 100 times that of the salinity, i.e., $\delta = 100$. Then the temperature difference between the two layers decreases faster than that of the salinity, such that the value of $R_\rho(t) = \frac{\alpha_T \Delta T}{\alpha_S \Delta S}$ keeps decreasing before the onset time. When the initial density stability ratio $R = R_{\rho 0}$ is greater, the system maintains in the diffusion period longer, i.e., the onset time is greater. Note that, $R_\rho(t)/R\rho 0$ decreases at the same rate before the onset time, which will be discussed later.

After the onset time, $\tau > \tau_o$, convection appears on the interface, and temperature and salinity are transported across the interface by 'density fingers' or 'salt fingers'. The value of $R_\rho(t)$ starts increasing and the whole system becomes more gravitationally stable. Note that we did not apply the constant temperature condition to the top and lower boundary, such that $R_\rho(t)$ will tend towards 1 when the hot salt water is fully mixed with the cold pure water. Hence $R_\rho(t)$ does not monotonically increase after the onset time, as was the case in Singh and Srinivasan (2014), in which the temperature stayed constant at the top and lower boundaries.

Table 1. Dimensionless onset time τ_o of convection.

	τ_o in a	τ_o in
$R = R_{\rho 0}$	Hele-Shaw cell	extended geometry
0.05	1.86e − 06	1.97e − 05
0.25	1.04e − 05	6.85e − 05
0.8	4.29e − 05	2.02e − 04
1	5.68e − 05	2.61e − 04
4	5.11e − 04	1.39e − 03
20	> 2.57e − 02	> 3.68e − 03

The Hele-Shaw cell

The time sequences of the temperature T, salinity S and horizontally averaged $< T,S >$ fields of thermohaline stratification in the Hele-Shaw cell at $Ra_T = 7 \cdot 10^6$ with $R_{\rho 0} = 0.05, 0.25, 0.8, 1, 4, 20$ are shown in Figure 2. The three snapshots of temperature and salinity only show the left-hand panel of the whole domain. Three snapshots for averaged $< T,S >$ are plotted versus the vertical axis.

Obviously, when R increases, the boundary of the fingers becomes more blurred in both the temperature and salinity snapshots due to the diffusivity of temperature and salinity. Because $R_\rho(t)/R_\rho 0$ decreases at the same rate before the onset time, $< T,S >$ drops down further during $\tau \le \tau_o$, where τ_o is greater for thermohaline stratification with a greater R. After the onset time, convection begins to govern the flow dynamics and slim fingers begin to appear on the interface. Then temperature and salinity are transported along the fingers vertically. Additionally, the diffusivity coefficient of the temperature is 100 times

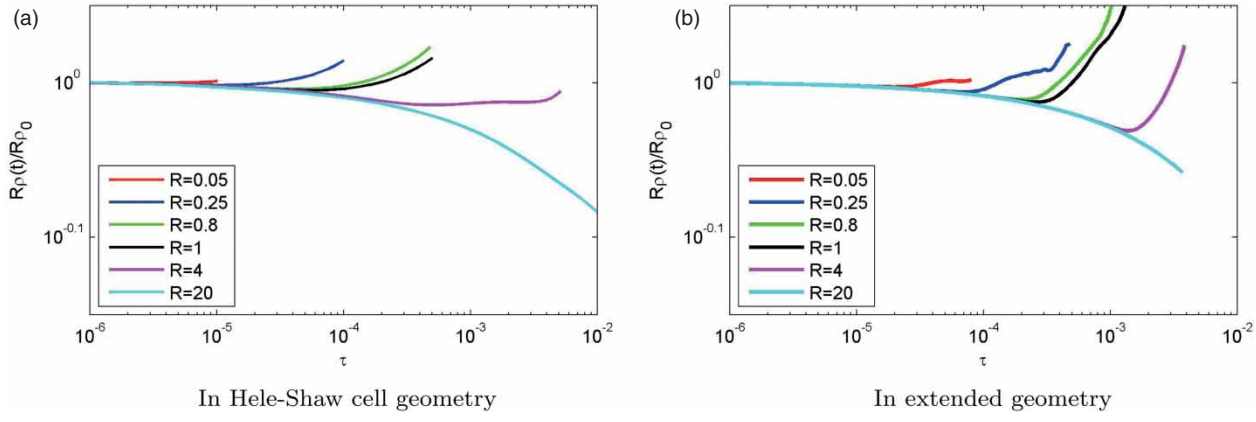

Figure 1. . Variation of $R_\rho(t)/R_{\rho 0}$ as a function of τ with different values of the initial density stability ratio $R_{\rho 0}$.

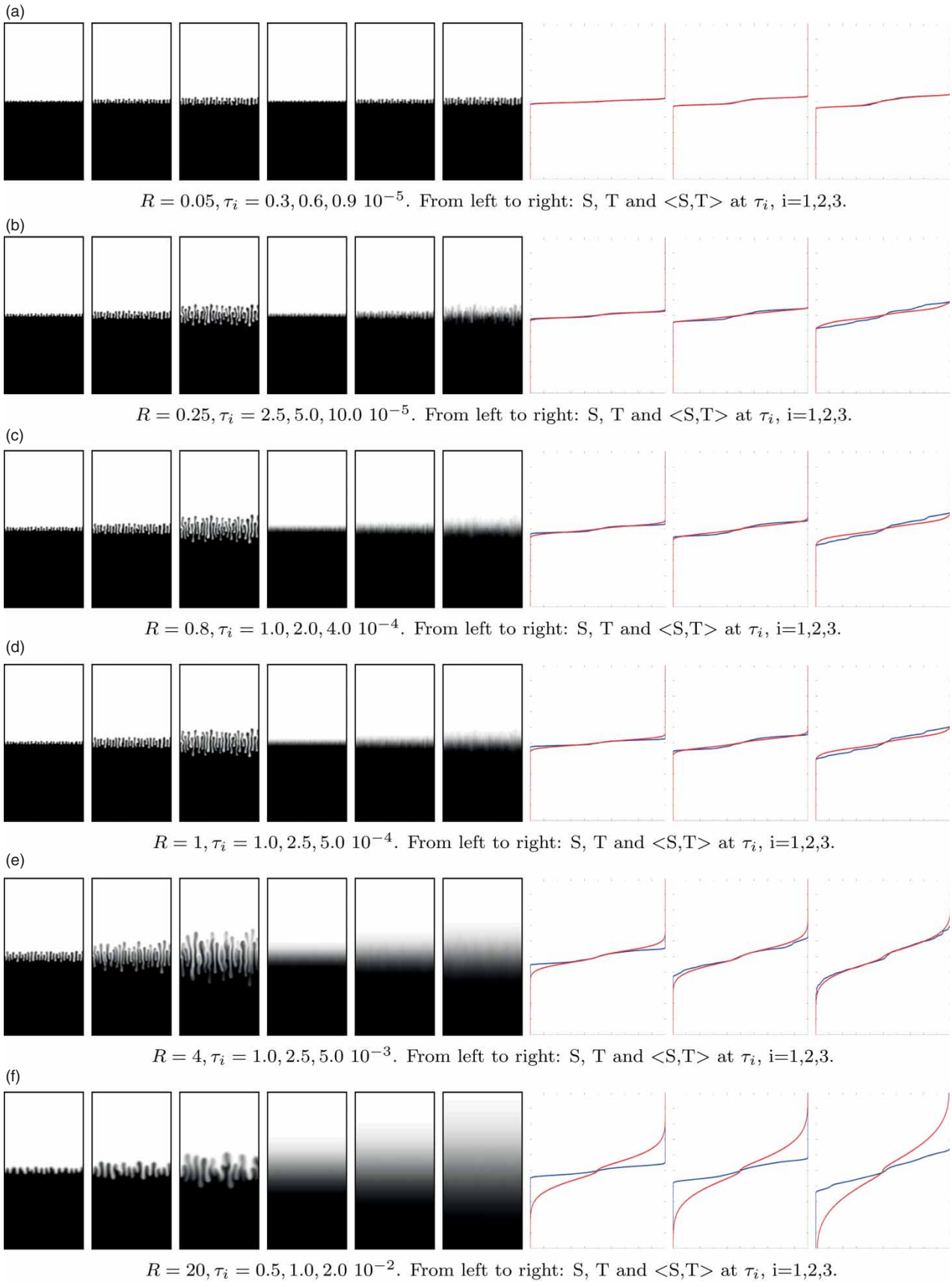

Figure 2. Time evolution of the temperature T, salinity S and horizontally averaged values $< T,S >$ for thermohaline stratification in a Hele-Shaw cell with $\delta = 0.01$ and $\Theta = 10^{-4}$ at a high thermal Rayleigh number of $Ra_T = 7{\cdot}10^6$: In the last three columns, the horizontally averaged values of temperature, $< T >$, are shown by red lines, while salinity values $< S >$ are shown by blue lines.

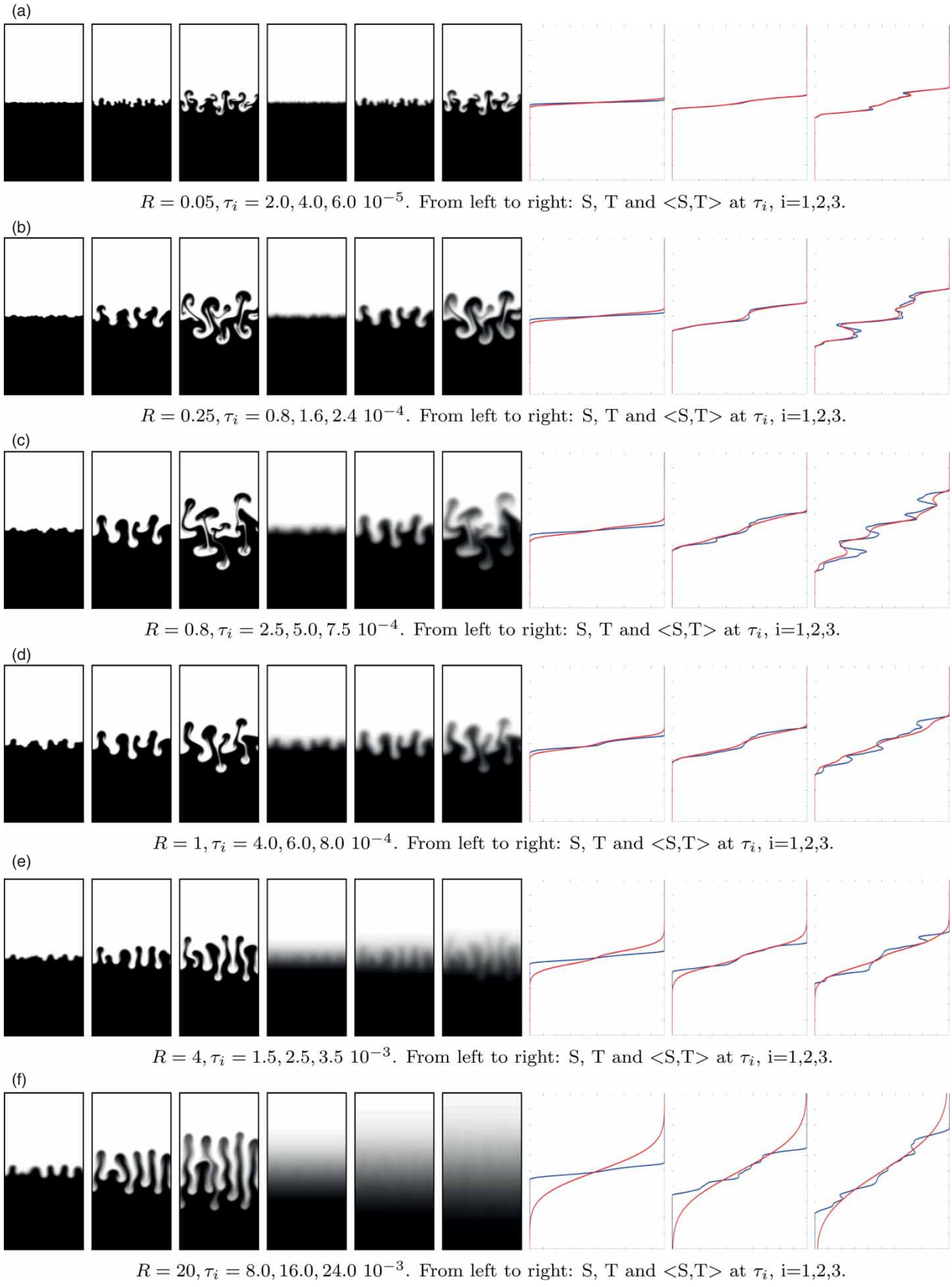

Figure 3. Time evolution of the temperature T, salinity S and horizontally averaged values $< T,S >$ for thermohaline stratification in extended geometry with $\delta = 0.01$ at a high thermal Rayleigh number of $Ra_T = 7{\cdot}10^6$: In the last three columns, the horizontally averaged values of temperature, $< T >$, are shown by red lines, while salinity values $< S >$ are shown by blue lines.

that of the salinity, so the temperature snapshots are more blurred than those of salinity.

When $R < 1$, the onset time is small such that T and S change much less in the diffusion regime. Hence, we observed nearly the same T and S at $R = 0.05$ in Figure 1. After the onset time, the heat and mass transfer along the density fingers, driven by RT instability. When $R > 1$, the onset time is much greater, and salt fingers with blurring interface driven by DD instability appear even before the onset time of convection, as shown in Figure 2(f).

Extended geometry

Figure 3 shows the time sequences of the temperature T, salinity S and horizontally averaged $< T,S >$ fields of thermohaline stratification in extended geometry. Again, the three snapshots for temperature and salinity only show the left-hand panel of the whole domain, and the three snapshots for averaged $< T,S >$ are plotted versus the vertical axis. We observed a similar tendency as discussed above: ΔT and ΔS decrease to a lower value in the longer diffusive regime, such that the finger boundary becomes more blurred for larger values of R.

In extended geometry, Darcy's law fails, and the flow dynamics are governed by the Navier-Stokes equation with the nonlinear momentum convection term. Then, the fingers grow up almost linearly after the onset time, and large-scale shearing convection appears in the mixed layers. Strong horizontal shear detaches the twisted fingers, and uniform concentration distribution is reached with the decreasing of the fingers (Singh & Srinivasan, 2014). In Figure 3, the fluctuation in the $< T,S >$ curve is due to the twisted fingers.

Base state density

In the study of Trevelyan et al. (2011), the base state density profile is defined as $< S > /R - < T >$, and the theoretical solution is obtained based on the linear stability analysis. Here, the value of the base state density

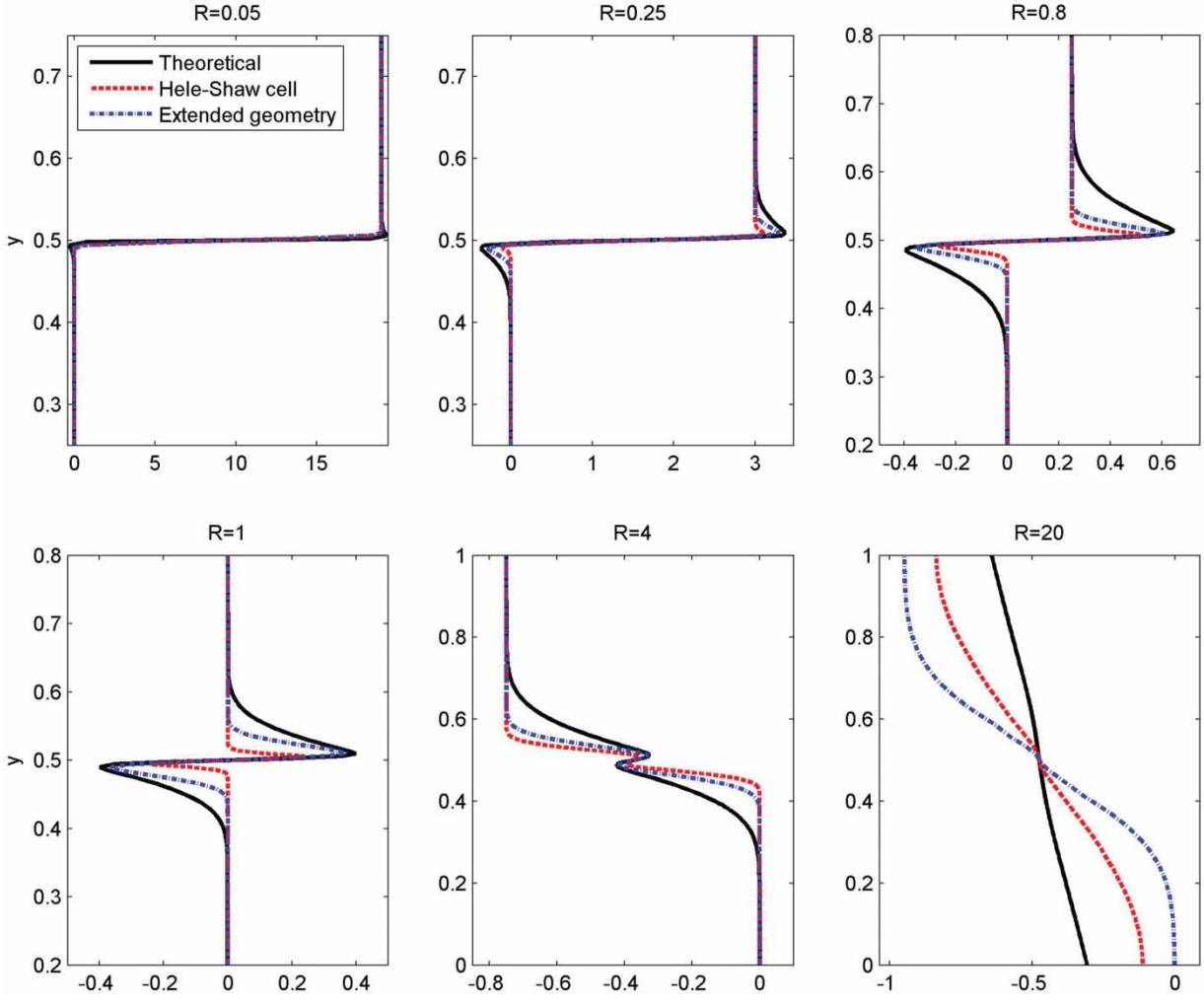

Figure 4. Base state density profile $\langle S \rangle / R - \langle T \rangle$ versus vertical axis in diffusive regime. Black: Theoretical result (Trevelyan et al., 2011); Red: in a Hele-Shaw cell; Blue: in extended geometry.

profile is calculated using the horizontally averaged numerical solution of temperature and salinity at the time $\tau \simeq \tau_o/2$. Figure 4 shows that the base state density of thermohaline stratification in extended geometry is very similar to that of a Hele-Shaw cell.

The classification of buoyancy-driven instabilities in (R, δ) space for miscible two-layer flow satisfying Darcy's law is based on the theoretical solution of the base state density profile from linear stability analysis (Trevelyan et al., 2011). For cases with $R \leq 1$ in Figure 4, all density profiles contain two local extrema and belong to the same region in (R, δ) space (Trevelyan et al., 2011). For the case where $R = 4$, classified into the region $\delta > R^2 > 1$, all density profiles contain a local strategically stable region near the interface. For the case where $R = 20$, classified into the region $R^2 > \delta > 1$, all density profiles monotonously increase downwards, indicating gravitational stability. The base state density profiles are always in the same form whether the flow dynamics satisfy Darcy's law or not. Hence, it can be claimed that the classification of buoyancy-driven instabilities in (R, δ) space for miscible two-layer stratifications in the Hele-Shaw cell can be extended to the unbounded stratifications.

Conclusion

This study compared buoyancy-driven instabilities for thermohaline stratification ($\delta = 100$) in a Hele-Shaw cell and in extended geometry. For unbounded thermohaline stratification in extended geometry, the fingers are twisted by the nonlinear momentum convection, leading to stronger turbulence and quicker concentration transfer. In a Hele-Shaw cell, the fingers are slimmer and straighter, and the onset time of convection is much smaller than that of the comparative case in extended geometry. Nonetheless, the base state density profile of thermohaline stratification in extended geometry is similar to that of a Hele-Shaw cell; hence, the classification of buoyancy-driven instabilities in (R, δ) space for flow in a Hele-Shaw cell can be extended to the unbounded thermohaline stratification.

Additionally, when the density stability value R is greater, the onset time of the convection is larger, and temperature and salinity transfer at a slower rate and in a different ratio during the diffusion regime. As the density stability ratio R decreases, the onset time shortens such that the flow dynamics are governed by density fingers sooner, which are found to transfer heat and mass faster compared to salt fingers.

Disclosure statement

No potential conflict of interest was reported by the authors.

Funding

This work was supported by the National Natural Science Foundation of China project [40906006].

References

Carballido-Landeira, J., Trevelyan, P. M. J., Almarcha, C., & De Wit, A. (2013). Mixed-mode instability of a miscible interface due to coupling between rayleigh-taylor and double-diffusive convective modes. *Physics of Fluids*, *25*(2). Retrieved from http://dx.doi.org/10.1063/1.4790192

Fernandez, J., Kurowski, P., & Petitjeans, P. (2002). Density-driven unstable flows of miscible fluids in a Hele-Shaw cell. *Journal of Fluid Mechanics*, *451*, 239–260.

Griffiths, R. (1981). Layered double-diffusive convection in porous media. *Journal of Fluid Mechanics*, *102*, 221–248.

Li, Y.-S., Zhan, J.-M., & Luo, Y.-Y. (2008). Unsteady phenomena in the double-diffusive convection flows at high rayleigh number. *Numerical Heat Transfer, Part A: Applications*, *54*(11), 1061–1083.

McLean, J., & Saffman, P. (1981). The effect of surface tension on the shape of fingers in a Hele Shaw cell. *Journal of Fluid Mechanics*, *102*, 455–469.

Mishra, M., Trevelyan, P. M. J., Almarcha, C., & De Wit, A. (2010). Influence of double diffusive effects on miscible viscous fingering. *Physical Review Letters*, *105*, 204501.

Radko, T. (2008). The double-diffusive modon. *Journal of Fluid Mechanics*, *609*, 59–85.

Radko, T., & Stern, M. E. (2000). Finite-amplitude salt fingers in a vertically bounded layer. *Journal of Fluid Mechanics*, *425*, 133–160.

Rongy, L., Trevelyan, P. M. J., & De Wit, A. (2010). Influence of buoyancy-driven convection on the dynamics of $A + B \rightarrow C$ reaction fronts in horizontal solution layers. *Chemical Engineering Science*, *65*(7), 2382–2391.

Sharp, D. (1983). An overview of rayleigh-taylor instability. In: Fronts, Interfaces and Patterns. Proceedings of the Third Annual International Conference of the Centre for Nonlinear Studies. Vol. 12D of Physica. Los Alamos, NM, USA, pp. 3–18.

Singh, O. P., & Srinivasan, J. (2014). Effect of rayleigh numbers on the evolution of double-diffusive salt fingers. *Physics of Fluids*, *26*, 062104. Retrieved from http://dx.doi.org/10.1063/1.4882264

Stern, M. E. (1960). The 'salt-fountain' and thermohaline convection. *Tellus*, *12*, 172–175.

Stern, M. E., & Radko, T. (1998). The salt finger amplitude in unbounded T-S gradient layers. *Journal of Marine Research*, *56*, 157–196.

Stern, M. E., & Simeonov, J. (2005). The secondary instability of salt fingers. *Journal of Fluid Mechanics*, *533*, 361–380.

Trevelyan, P., Almarcha, C., & De Wit, A. (2011). Buoyancy-driven instabilities of miscible two-layer stratifications in porous media and Hele-Shaw cells. *Journal of Fluid Mechanics*, *670*, 38–65.

Yoshida, J., & Nagashima, H. (2003). Numerical experiments on salt-finger convection. *Progress in Oceanography 56*(3–4), 435–459.

Zhan, J. M., Luo, Y. Y., & Li, Y. S. (2008). A high accuracy hybrid method for two-dimensional Navier–Stokes equations. *Applied Mathematical Modelling*, *32*, 873–888.